

# Finite-Difference Time-Domain Study of Guided Modes in Nano-plasmonic Waveguides

Yan Zhao, *Student Member, IEEE*, and Yang Hao, *Senior Member, IEEE*

**Abstract**—The finite-difference time-domain (FDTD) method is applied for studying plasmonic waveguide formed by silver nanorods at optical frequencies. The dispersion diagram of periodic structures formed by an infinite number of nanorods is calculated by applying Bloch's periodic boundary condition therefore only one unit-cell is modelled in simulations. The frequency dispersion of silver nanorods is characterised by Drude material model and taken into account in FDTD simulations by a simple differential equation method. The dispersion diagram calculated using the FDTD method is verified by comparing the frequency domain embedding method. The change of dispersion diagram caused by the elliptical inclusion and different number of rows of nanorods is analysed. Wave propagation in the waveguides formed by a finite number (nine) of nanorods is studied and the transmission for different waveguides is calculated and compared with the corresponding dispersion diagrams. The simulation results show that row(s) of nanorods can guide the propagation of light due to the coupling of surface plasmon. However, only certain guided modes exist in these plasmonic waveguides but higher guided modes are hard to be excited in finite plasmonic waveguides.

## I. INTRODUCTION

It is well known that the photonic crystals (PCs) offer unique opportunities to control the flow of light [1]. The basic idea is to design periodic dielectric structures that have a bandgap for a particular frequency range. Periodic dielectric rods with removed one or several rows of elements can be used as waveguiding devices when operating in the bandgap frequencies. A lot of effort has been made in order to obtain a complete and wider bandgap. It has been shown that a triangular lattice of air holes in a dielectric background has a complete bandgap for TE (transverse electric) polarization, while a square lattice of dielectric rods in air has a bandgap for TM (transverse magnetic) polarization [2]. On the other hand, the devices operating in the bandgap frequencies are not the only option to guide the flow of light. Another waveguiding mechanism is the total internal reflection (TIR) in one-dimensional (1-D) periodic dielectric rods [3]. It is analysed in [3] that a single row of dielectric rods or air-holes supports waveguiding modes and therefore also can be used as waveguide. In [4], the design of such waveguides consisting of several rows of dielectric rods with various spacings is proposed.

Another type of waveguide in optical frequency range has also drawn a lot of attention because of its ability of transporting energy with concentration of light below the diffraction limit. The transport of energy in such a kind of waveguide is based on the coupling of surface plasmons. Previous analysis of surface plasmons includes the plasmon propagation along

metal stripes, wires, or grooves in metal [5]–[10], and also the coupling between plasmons on metal particles in order to guide energy is investigated [11], [12]. In [13], the optical pulse propagation below the diffraction limit is shown using the finite-difference time-domain (FDTD) method. Also with the FDTD method, the waveguide formed by several rows of silver nanorods arranged in hexagonal is studied [14].

The aforementioned subwavelength structures can also find their applications at microwave frequencies. Recently composite materials [15] were designed containing randomly distributed electrically conductive material and non-electrically conductive material. They were noted exhibiting plasma-like responses at frequencies well before plasma frequencies of the bulk material.

In this paper, we study the properties of 1-D plasmonic waveguide formed by one or two rows of nanorods. Section II introduces detailed FDTD calculation of dispersion diagram for 1-D periodic structures. In section III, we analysis wave propagation in the waveguide formed by a finite number of elements. Section IV concludes the paper.

## II. FDTD CALCULATIONS OF DISPERSION DIAGRAM

The finite-difference time-domain (FDTD) method has been widely used for modelling of transient wave propagation in frequency dispersive and non-dispersive media [16]. Furthermore, applying appropriate boundary conditions (e.g. Bloch's periodic boundary conditions (PBCs)), FDTD method can be used to calculate dispersion diagram for periodic structures and therefore only one unit-cell of the two-dimensional (2-D) or three-dimensional (3-D) infinite structure is necessary in calculations [17], [18]. For any periodic structures, the field at any time should satisfy the Bloch theory, i.e.

$$\mathbf{E}(d + \mathbf{L}) = \mathbf{E}(d)e^{j\mathbf{kL}}, \quad \mathbf{H}(d + \mathbf{L}) = \mathbf{H}(d)e^{j\mathbf{kL}}, \quad (1)$$

where  $d$  is any location in the computation domain,  $\mathbf{k}$  is the wave vector and  $\mathbf{L}$  is the lattice vector along the direction of periodicity. When updating the fields at the boundary of the computation domain using the FDTD method, the required fields outside the computation domain can be calculated using the known field value inside the domain through Eq. (1).

For 1-D periodic structures, the absorbing boundary conditions (ABCs) are required to truncate simulation domain in order to minimize reflections from outer boundaries. The perfectly matched layer (PML) proposed by Berenger [19] as one of the most effective ABCs, is proven to only introduce reflections as low as -120 dB. For the study of 1-D plasmonic waveguides performed in this paper, the Bloch's PBCs are

applied at the boundaries along  $x$ -direction and Berenger's original split-field PMLs are used to terminate the simulation domain along  $y$ -direction (see Fig. 1).

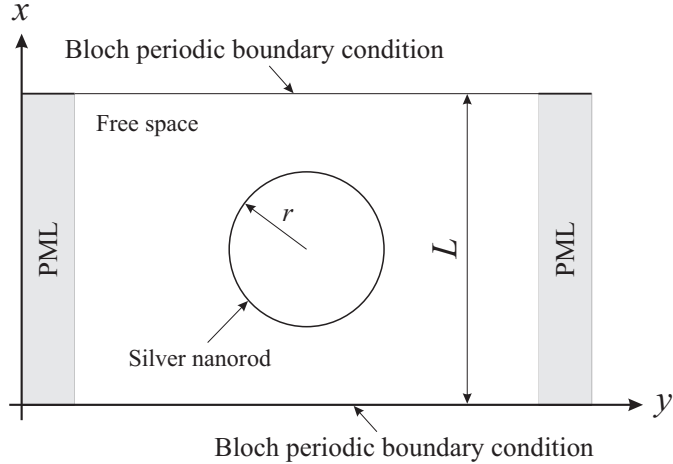


Fig. 1. The layout of the 2-D FDTD computation domain for calculating dispersion diagram for 1-D periodic structures. The inclusion has a circular cross-section with radius  $r$  and the period of the 1-D infinite structure is  $L$ .

The silver nanorods at optical frequency range can be characterised by Drude material model with the frequency dependent relative permittivity given by

$$\varepsilon(\omega) = 1 - \frac{\omega_p^2}{\omega^2 - j\omega\gamma}, \quad (2)$$

where  $\omega_p$  is the plasma frequency and the  $\gamma$  is the collision frequency which also defines the loss of the material. Conventional FDTD method updates electric field  $\mathbf{E}$  and magnetic field  $\mathbf{H}$  at each half time-step using the leapfrog scheme. In order to take into account the frequency dispersion of the material, the electric flux density  $\mathbf{D}$  is introduced into standard FDTD updating equations. At each time step,  $\mathbf{D}$  is updated directly from  $\mathbf{H}$  and  $\mathbf{E}$  can be calculated from  $\mathbf{D}$  using a simple finite-difference scheme applying inverse Fourier transformation, i.e.  $j\omega \rightarrow \partial/\partial t$  and  $\omega^2 \rightarrow -\partial^2/\partial t^2$ .

The FDTD simulation domain is represented by an equally spaced three-dimensional (3-D) grid with periods  $\Delta_x$ ,  $\Delta_y$  and  $\Delta_z$  along  $x$ -,  $y$ - and  $z$ -directions, respectively. The discrete time step is denoted as  $\Delta_t$ . Then the updating equation for  $\mathbf{E}$  in terms of  $\mathbf{E}$  and  $\mathbf{D}$  at previous time steps is as follows:

$$\begin{aligned} \mathbf{E}^{n+1} = & \left\{ \left( \frac{1}{\Delta_t^2} + \frac{\gamma}{2\Delta_t} \right) \mathbf{D}^{n+1} - \frac{2}{\Delta_t^2} \mathbf{D}^n \right. \\ & + \left( \frac{1}{\Delta_t^2} - \frac{\gamma}{2\Delta_t} \right) \mathbf{D}^{n-1} - \left[ \varepsilon_0 \left( -\frac{2}{\Delta_t^2} + \frac{\omega_p^2}{2} \right) \mathbf{E}^n \right. \\ & \left. \left. + \varepsilon_0 \left( \frac{1}{\Delta_t^2} - \frac{\gamma}{2\Delta_t} + \frac{\omega_p^2}{4} \right) \mathbf{E}^{n-1} \right] \right\} / \varepsilon_0 \left( \frac{1}{\Delta_t^2} + \frac{\gamma}{2\Delta_t} + \frac{\omega_p^2}{4} \right). \end{aligned} \quad (3)$$

Note that if the plasma frequency is set to zero, i.e.  $\omega_p = 0$ , the above dispersive FDTD formulation (4) reduces to the updating equation in free space.

The dispersion diagram of periodic structures gives the relation between the frequency and the wave vector. In FDTD calculations, wide-band Gaussian pulses covering the

frequency range of interest are used as source excitations. Then the directly obtained time-domain response is Fourier transformed into the frequency domain where the location of each peak corresponds to the resonance frequency for a given wave vector. In order to capture all possible resonant modes of the structure, the signals at one hundred randomly selected locations are recorded, transformed into the frequency domain and combined in order to obtain the dispersion diagram.

In this paper, we study the plasmonic waveguides formed by a single row or two rows of infinite number of circular nanorods, therefore a 2-D simulation domain can be used and the TE mode with respect to the simulation domain is considered.

Since the conventional FDTD uses staircasing to approximate curved structures, in order to investigate the numerical accuracy of the FDTD method for our applications, we have performed two sets of simulations with different spatial resolutions i.e. FDTD cell sizes:  $\Delta_x = \Delta_y = 2.5$  nm and  $\Delta_x = \Delta_y = 1.0$  nm which give 60 and 150 cells per free space wavelength at the highest normalised frequency of interest 0.5 ( $\bar{f} = \omega L/2\pi c$ , where  $c$  is the speed of light in free space), respectively. The time step is calculated as  $\Delta_t = \Delta_x/\sqrt{2}c$  according to the stability criterion [16]. The plasma frequency in (2) is  $\omega_p = 9.39 \times 10^3$  THz. The collision frequency has to be properly chosen so that the peaks in the spectrum do not disappear because of the losses in material, and also the convergence of simulations can be improved. In our simulations, the collision frequency is chosen as  $\gamma = 0.032\omega_p$  which is based on numerical analysis and the comparison with frequency domain embedding method [22]. The radius of the cylindrical nanorods is 25.0 nm and the period of the infinite structure is 75.0 nm. Wide-band Gaussian-shaped impulses are used as source excitations in order to cover the whole frequency range of interest ( $\bar{f} = 0 \sim 0.5$ ):

$$g(t) = e^{-\left(\frac{t-t_0}{\tau}\right)^2} \cdot e^{j\omega t} \quad (4)$$

where  $t_0$  is the initial time delay,  $\tau$  defines the pulse width and  $\omega$  is the centre frequency of the pulse ( $\bar{f} = 0.25$ ).

As illustrated in Fig. 1, the computation domain contains one period along  $x$ -direction. Along  $y$ -direction, additional cells for the free-space are added in order to improve the performance of PMLs since the calculation of dispersion diagram requires very accurate absorbing boundaries. The simulation results are then compared with the frequency domain embedding method [22]. Fig. 2 shows the dispersion diagram for a plasmonic waveguide formed by a single row of infinite number of cylindrical nanorods. It can be seen that the case for  $\Delta_x = 1.0$  nm shows good agreement with the frequency domain embedding method, while lower spatial resolution (larger cell size,  $\Delta_x = 2.5$  nm) causes the shift of resonant frequencies. In the following analysis, we keep  $\Delta_x = 1.0$  nm for all the rest of simulations. It's also worth mentioning that the embedding method gives more accurate results due to that the calculation of the detailed flat bands is beyond the ability of the conventional FDTD method. However, the advantage of the FDTD method is that the geometries of arbitrary shapes can be modelled. For the case of  $\Delta_x = 1.0$  nm, the field patterns (amplitude) corresponding to different modes at normalised

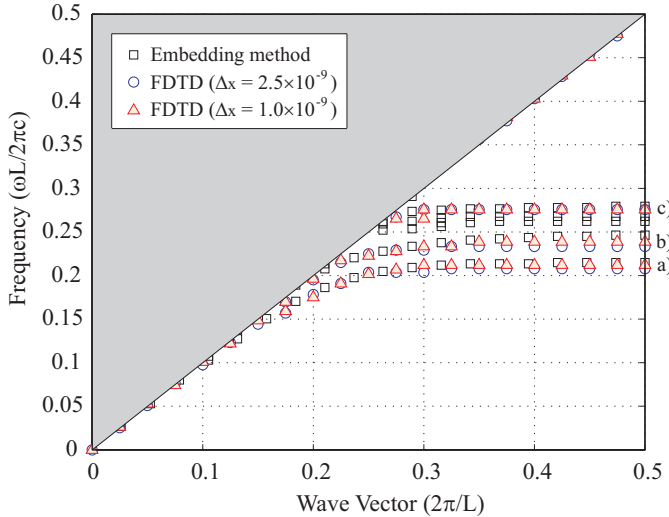


Fig. 2. Comparison of dispersion diagram calculated from dispersive FDTD simulations using different spatial resolutions (FDTD cell size) and the frequency domain embedding method for 1-D periodic nanorods. Only the region for guided modes is shown.

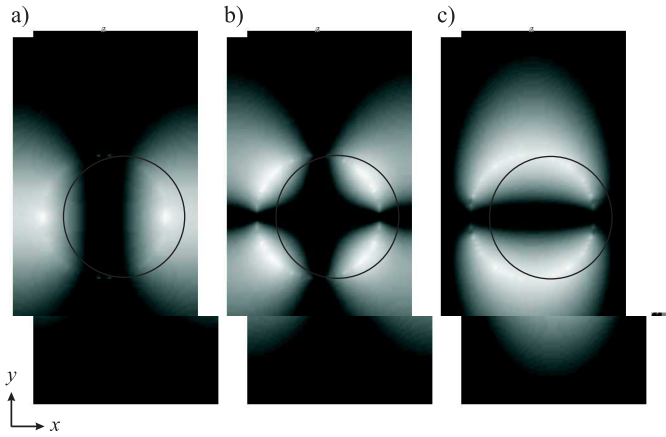


Fig. 3. The distribution of magnetic field corresponding to different guided modes as marked in Fig. 2. a) transverse mode; b) hybrid mode and c) longitudinal mode

wave number  $k_x = 0.5$  as marked in Fig. 2 are plotted in Fig. 3. It can be seen that the field changes the polarisation from the point a) to point c) in Fig. 2, and the field at point b) represents a hybrid mode. Note that when calculating these field distributions as well as those for the waveguides formed by a finite number of elements in the next section, the collision frequency is set to zero ( $\gamma = 0$ ) in order to reach steady-state in simulations.

Using the FDTD method, we also study the dispersion diagrams of different plasmonic waveguides formed by a single row of infinite number of elliptical nanorods and two rows of infinite number of circular nanorods arranged in square lattice. The elliptical element has a ratio of semimajor-to-semiminor axis 2:1, where the semiminor axis is equal to the radius of the circular element (25.0 nm). For the two rows of circular nanorods, the spacing between two rows (centre-to-centre distance) is 75.0 nm. The dispersion diagrams for these infinite structures are plotted in Figs. 4 and 6. It can be

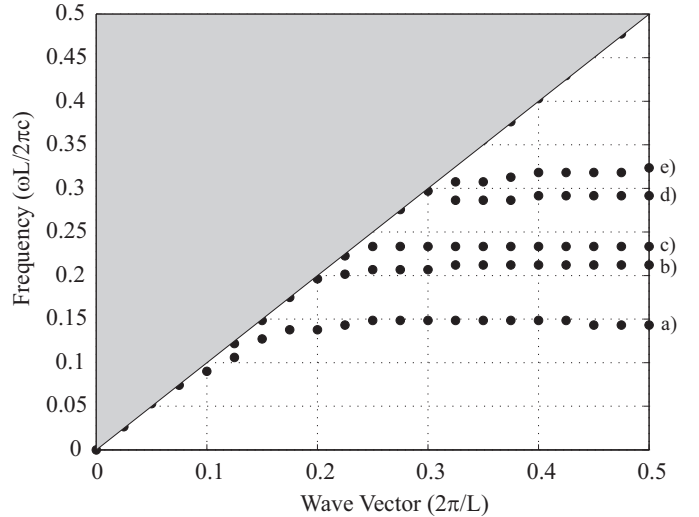


Fig. 4. Dispersion diagrams for a single row of elliptical nanorods calculated from dispersive FDTD simulations.

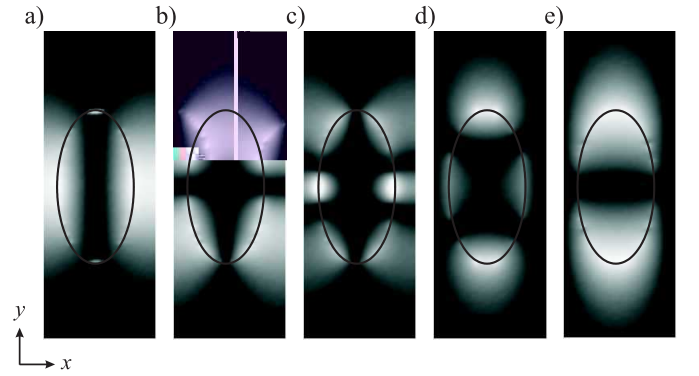


Fig. 5. The distribution of magnetic field corresponding to different guided modes as marked in Fig. 4.

seen in Fig. 4 that the dispersion curves have been modified by changing the inclusion element. Comparing to the circular inclusion, the dispersion curves become more separated to occupy wider bandwidth and additional guided modes appear for the elliptical inclusion. Figs. 5a, b and e correspond to the field distribution in Fig. 3a, b and c for circular inclusion, respectively. And Figs. 5c and d are the two additional modes introduced by changing from circular to elliptical inclusion.

The dispersion diagram for the two-circular inclusion is shown in Fig. 6. The dispersion curves are only slightly modified by adding one more circular element. However, one more guided mode appears due to the coupling of two-circular elements. Such phenomenon was also found in dielectric nanorods previously [4]. In Fig. 7, the magnetic field distribution shows different guided modes corresponding to the frequencies as marked in Fig. 6. We can see the strong coupling between the two silver nanorods. Again Figs. 7a, c and d have similar distributions as Figs. 3a, b and c, respectively, and Fig. 7b is the extra mode caused by the coupling between two nanorods.

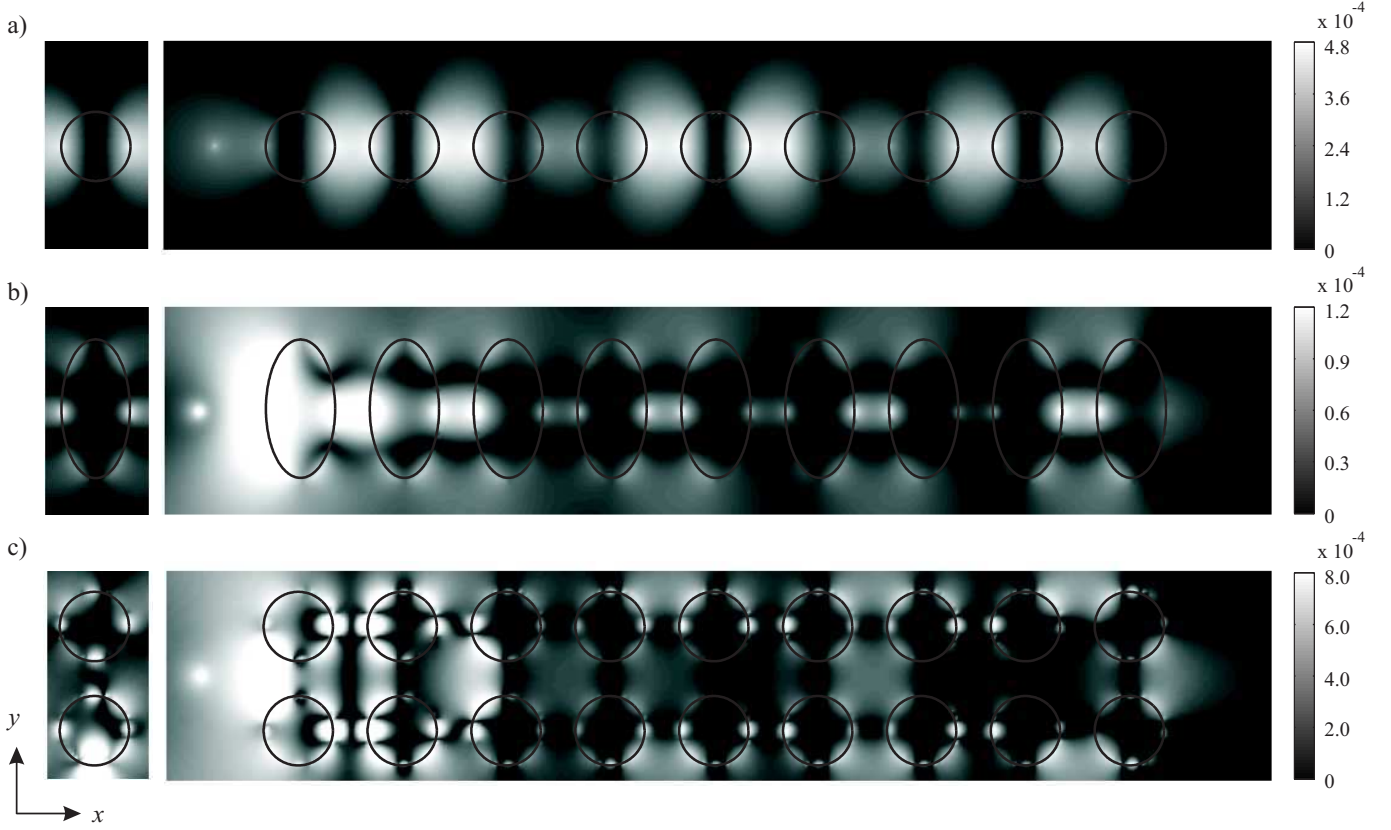


Fig. 8. Distributions of magnetic field corresponding to different guided modes for nine-element plasmonic waveguides formed by a) a single row of circular nanorods (a point in Fig. 2) b) a single row of elliptical nanorods (b point in Fig. 4) c) two rows of circular nanorods arranged in square lattice (c point in Fig. 6). The number of elements in waveguides is nine. The corresponding field distribution of guided modes in infinite structures are shown on the left side of the figure.

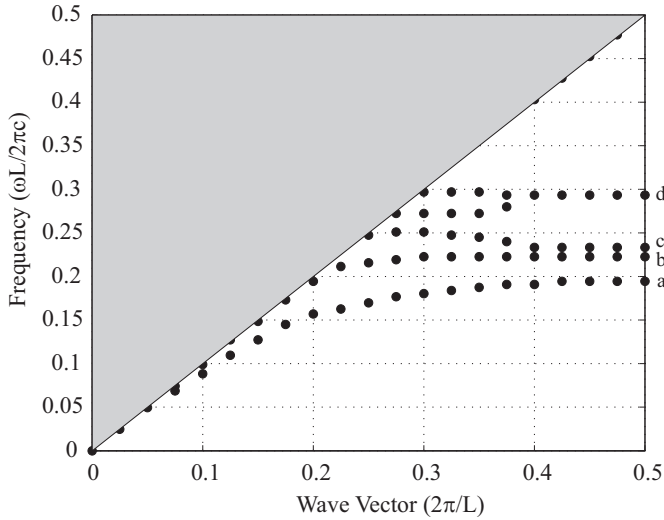


Fig. 6. Dispersion diagrams for two rows of circular nanorods arranged in square lattice calculated from dispersive FDTD simulations.

### III. WAVE PROPAGATION IN PLASMONIC WAVEGUIDES

In order to study wave propagation in plasmonic waveguides formed by a finite number of nanorods, we remove the PBCs and place PMLs at all four outer boundaries of the simulation domain. Again additional free-space FDTD cells are also added into the simulation domain along the  $x$

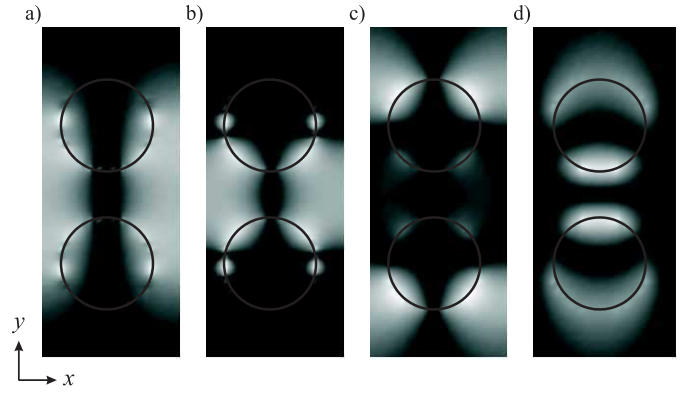


Fig. 7. The distribution of magnetic field corresponding to different guided modes as marked in Fig. 6.

direction for better performance of the PMLs. The number of nanorods under study is nine. The spacing (pseudo-period) between adjacent elements remains the same as for the infinite structures in the previous section. For single-mode excitation, we choose the frequency of the corresponding mode from the dispersion diagram, and excite the sinusoidal source from one end of the waveguides. Fig. 8 shows magnetic field patterns for different waveguides operating in different guided modes. The field plots are taken after the steady-state has been reached in simulations. On the left side of the figure, the

guided modes in infinite structures are plotted for different waveguides. It is clearly seen that the single guided mode is coupled into the plasmonic waveguides formed by a finite number of elements. Fig. 8 illustrates only certain modes can be excited in plasmonic waveguides formed by finite number of nanorods.

By changing the operating frequency, we analyse whether or not other high order guided modes exist in finite-element waveguides. Fig. 9 shows the magnetic field distribution (amplitude) in the nine-element waveguide at higher guided modes (e.g. c point in Fig. 2). The corresponding higher guided modes in infinite structures are also plotted on the left for comparison. It can be seen that these higher modes exist

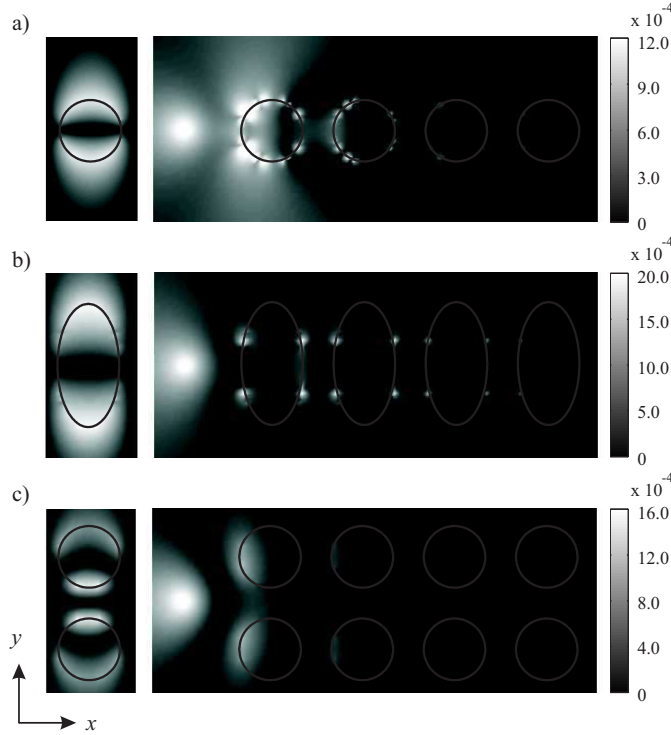


Fig. 9. Distributions of magnetic field showing that the corresponding highest guided modes (c, e and d points in Figs. 2, 4 and 6 respectively) in infinite periodic structures are not excited in the nine-element plasmonic waveguides formed by a) a single row of circular nanorods b) a single row of elliptical nanorods c) two rows of circular nanorods arranged in square lattice.

in infinite structures but are not excited in finite plasmonic waveguides. On the other hand the incident wave excites other modes which decay along the waveguide and do not account for the guiding of waves. Such phenomenon can be understood from the analysis of transmission through these waveguides.

For calculation of transmission through the waveguide, the Gaussian-shaped pulse (4) is used and excited at a distance of 60.0 nm from one end of the waveguides. The total-field/scattered-field method [16] is used in order to simulate the plane-wave normal incidence on the waveguides. Time-domain fields are recorded by input and output detectors placed at different ends of the waveguide. The incident wave is taken when the waveguides are removed from the simulation domain, i.e. the free space situation. The transmission are then obtained by transforming time domain fields into the

frequency domain and calculating the ratio of transmitted field to incident field. Fig. 10 shows the transmission through the

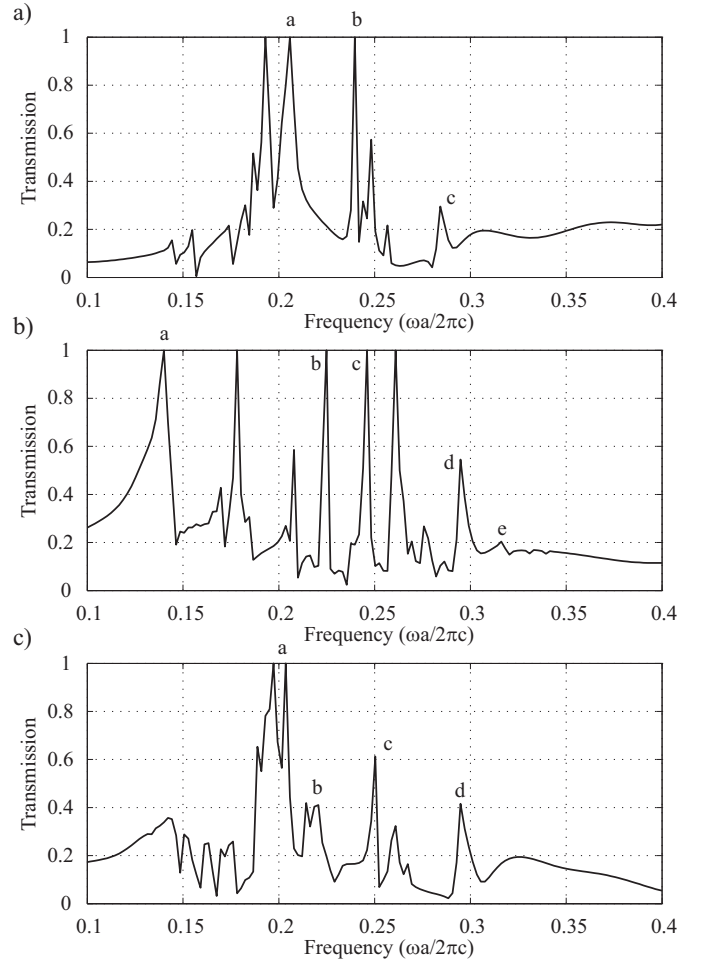


Fig. 10. Transmission coefficients through nine-element plasmonic waveguides formed by a) one row of circular nanorods b) one row of elliptical nanorods c) two rows of circular nanorods calculated using the total-field/scattered-field method and plane wave normal incidence from dispersive FDTD simulations. The corresponding guided modes in Figs. 2, 4 and 6 are marked as a, b, ... e, respectively.

waveguides formed by nine nanorods with different elements as inclusions. It can be seen the maximum transmission happens at the locations corresponding to the position in the dispersion diagram, which indicates that these guided modes are indeed excited in finite-element plasmonic waveguides. The slightly shifts of these peak locations to lower frequencies may be due to the finite number of nanorods in waveguides. However, low transmission occurs at the location of higher guided modes, which explains the the field distribution results in Fig. 9. Some sparks in Fig. 10 cannot be identified from dispersion diagrams (Figs. 2, 4 and 6) and it can be explained that multiple Fabry-Perot resonances occur from nanorods in the waveguide with finite length.

Compared to the conventional plasmonic waveguide with circular inclusions, the waveguide composed of elliptical nanorods demonstrate lower fundamental modes and multiple transmission peaks in the frequency range ( $\omega L/2\pi c$ ) below 0.3. When two rows of circular inclusions formed in a square

lattice are considered as a waveguide, the transmission curve shows the first two transmission peaks are degenerated and hence potential wideband plasmonic waveguide can be created by structure optimisation in such a configuration.

#### IV. CONCLUSIONS

In conclusion, we have performed dispersive FDTD simulations for calculating dispersion diagrams for infinite periodic structures, as well as modelling of plasmonic waveguides formed by a finite number of silver nanorods. The 1-D infinite structure is modelled by applying the Bloch periodic boundary condition. The frequency dispersion of the material is taken into account in FDTD modelling by using a simple differential equation method. The dispersion diagram calculated using the FDTD method is verified by comparing the frequency domain embedding method. The dispersion curves can be modified by changing the element (inclusion) of the infinite structure. By simulating the plasmonic waveguides formed by rows of nine nanorods we have found that lower guided modes in infinite structures exist in these waveguides but higher guided modes are difficult to be excited. The transmission analysis shows good correspondence to the dispersion diagram and verifies the observation for some fundamental modes. However, in the finite waveguides, extra resonances occur due to Fabry-Perot resonances and they are not predicted in the calculation of dispersion diagrams. In other words, a super-cell approach is needed in modelling practical plasmonic waveguides for engineering applications. Further work includes the investigation of the number of elements in plasmonic waveguides on the guided modes. Although results presented in this paper were focused at optical frequencies, with future advances in microwave plasmonic materials, novel applications can be found in the designs of small antenna and efficient absorbers.

#### ACKNOWLEDGMENT

The authors would like to thank Mr. N. Giannakis for providing simulation results using the embedding method.

#### REFERENCES

- [1] J. D. Joannopoulos, R. D. Meade, and J. N. Winn, *Photonic crystals: Molding the flow of light*, Princeton U. Press, Princeton, N.J., 1995.
- [2] G. Qiu, F. Lin, and Y. P. Li, "Complete two-dimensional bandgap of photonic crystals of a rectangular Bravais lattice," *Opt. Commun.*, vol. 219, pp. 285-288, 2003.
- [3] S. Fan, J. Winn, A. Devenyi, J. C. Chen, R. D. Meade, and J. D. Joannopoulos, "Guided and defect modes in periodic dielectric waveguides," *J. Opt. Soc. Am. B*, vol. 12, pp. 1267-1272, 1995.
- [4] D. Chigrin, A. Lavrinenko, and C. Sotomayor Torres, "Nanopillars photonic crystal waveguides," *Opt. Express*, vol. 12, pp. 617-622, 2004.
- [5] J. C. Weeber, A. Dereux, C. Girard, J. R. Krenn and J. P. Goudonnet, "Plasmon polaritons of metallic nanowires for controlling submicron propagation of light," *Phys. Rev. B*, vol. 60, pp. 90619068, 1999.
- [6] B. Lamprecht, J. R. Krenn, G. Schider, H. Ditlbacher, M. Salerno, N. Felidj, A. Leitner, F. R. Ausseregg, and J. C. Weeber, "Surface plasmon propagation in microscale metal stripes," *Appl. Phys. Lett.*, vol. 79, pp. 5153, 2001.
- [7] T. Yatsui, M. Kourogi, and M. Ohtsu, "Plasmon waveguide for optical far/near-field conversion," *Appl. Phys. Lett.*, vol. 79, pp. 45834585, 2001.
- [8] R. Zia, M. D. Selker, P. B. Catrysse, and M. L. Brongersma, "Geometries and materials for subwavelength surface plasmon modes," *J. Opt. Soc. Am. A*, vol. 21, pp. 24422446, 2004.
- [9] R. Charbonneau, N. Lahoud, G. Mattiussi, and P. Berini, "Demonstration of integrated optics elements based on long-ranging surface plasmon polaritons," *Opt. Express*, vol. 13, pp. 977984, 2005.
- [10] D. F. P. Pile, D. K. Gramotnev, "Channel plasmon-polariton in a triangular groove on a metal surface," *Opt. Lett.*, vol. 29, pp. 10691071, 2004.
- [11] M. Quinten, A. Leitner, J. R. Krenn, and F. R. Ausseregg, "Electromagnetic energy transport via linear chains of silver nanoparticles," *Opt. Lett.*, vol. 23, pp. 13311333, 1998.
- [12] M. L. Brongersma, J. W. Hartman, and H. A. Atwater, "Electromagnetic energy transfer and switching in nanoparticle chain arrays below the diffraction limit," *Phys. Rev. B*, vol. 62, pp. 1635616359, 2000.
- [13] S. A. Maier, P. G. Kik, and H. A. Atwater, "Optical pulse propagation in metal nanoparticle chain waveguides," *Phys. Rev. B*, vol. 67, pp. 205402, 2003.
- [14] W. M. Saj, "FDTD simulations of 2D plasmon waveguide on silver nanorods in hexagonal lattice," *Opt. Express*, vol. 13, no. 13, pp. 4818-4827, June 2005.
- [15] T. J. Shepherd, C. R. Brewitt-Taylor, P. Dimond, G. Fixter, A. Laight, P. Lederer, P. J. Roberts, P. R. Tapster, and I. J. Youngs, "3D microwave photonic crystals: Novel fabrication and structures," *Electron. Lett.*, vol. 34, pp. 787-789, 1998.
- [16] A. Taflove, *Computational Electrodynamics: The Finite Difference Time Domain Method*. Norwood, MA: Artech House, 1995.
- [17] S. Fan, P. R. Villeneuve and J. D. Joannopoulos, "Large omnidirectional band gaps in metalloelectric photonic crystals," *Phys. Rev. B*, vol. 54, pp. 11245-11251, 1996.
- [18] M. Qiu and S. He, "A nonorthogonal finite-difference time-domain method for computing the band structure of a two-dimensional photonic crystal with dielectric and metallic inclusions," *J. Appl. Phys.*, vol. 87, pp. 8268-8275, 2000.
- [19] J. R. Berenger, "A perfectly matched layer for the absorption of electromagnetic waves," *J. Computat. Phys.*, vol. 114, pp. 185-200, Oct. 1994.
- [20] F. B. Hildebrand, *Introduction to Numerical Analysis*. New York: McGraw-Hill, 1956.
- [21] Y. Zhao, P. Belov, and Y. Hao, "Modelling of wave propagation in wire media using spatially dispersive finite-difference time-domain method: numerical aspects," submitted to *IEEE Trans. Antennas Propagat.* (arXiv: cond-mat/0604012) (2006).
- [22] J. E. Inglesfield, "A method of embedding," *J. Phys. C: Solid State Phys.*, vol. 14, pp. 3795-3806, 1981.